# Density Functional Modeling of Double Exchange Interactions in Transition Metal Complexes. Calculation of the Ground and Excited State Properties of $[Fe_2(OH)_3(tmtacn)_2]^{2+}$

**Vincenzo Barone,[†] Alessandro Bencini,*[,‡] Ilaria Ciofini,[‡] Claude A. Daul,[§] and Federico Totti[‡]**

*Contribution from the Dipartimento di Chimica, Università di Napoli, Napoli, Italy, Dipartimento di Chimica, Università di Firenze, Firenze, Italy, and Institut de Chimie Inorganique et Analitique, Université de Fribourg, Pérolles, Fribourg, Switzerland*

*Received October 6, 1997. Revised Manuscript Received January 26, 1998*

**Abstract:** Density functional theory has been successfully applied to characterize the electronic structure and the magnetic properties of the mixed valence dinuclear complex $[Fe_2(OH)_3(tmtacn)_2]^{2+}$ modeled by replacing the tmtacn ligand with three ammonia molecules. Spectroscopic and magnetic properties have been computed in nice agreement with the experimental values. Minimum energy path calculations allowed us to compute the frequencies $\nu$ associated with the normal coordinate $Q_-$ responsible for the delocalization of the extra electron, and we present here a procedure for the full characterization of mixed valence transition metal dimers.

## Introduction

Transition metal complexes having two or more metal ions with noninteger oxidation numbers are generally called *mixed valence systems*, and their properties have been studied for many years.[1−3] Among the mixed valence clusters, those having ions with magnetic ground states have attracted the interest of solid state physicists and chemists for the possible use of these systems as molecular materials.[4] Further, mixed valence clusters are also found in a number of metalloenzymes containing iron, copper, and manganese where the presence of the metals in noninteger oxidation states was found to be of fundamental importance for the mechanisms of action of these enzymes.[5−7]

In transition metal homonuclear dimers having more than one unpaired electron, the mixed valence forces a spin-dependent electron-delocalization mechanism which can stabilize the spin state with the maximum spin multiplicity with respect to all the others. This effect is usually indicated with the term *double exchange*.[8−10] The magnetic properties of binuclear mixed valence compounds can be rationalized using a spin Hamiltonian which includes the usual superexchange isotropic constant, *J*, and the electron delocalization parameter, *B*.[11] In this formalism the energy of a state with total spin *S*, $E(S)$, takes the form

$$E_{\pm}(S) = \frac{J}{2}[S(S+1)] \pm B\left(S+\frac{1}{2}\right) \qquad (1)$$

where a positive *J* value means an antiferromagnetic exchange interaction. A positive value of the double exchange parameter *B*, which is related to the inter-ion electron transfer, always stabilizes the spin state with maximum spin $S = S_{max}$. This state can therefore be the ground state even if the electronic interactions which determine the value of *J* result in an overall antiferromagnetic contribution. The importance of this effect in the field of molecular magnetism is apparent. The effect of the double exchange interaction is that of doubling the number of spin levels: each spin state is split into one symmetric and one antisymmetric spin component, $E_{\pm}(S)$. In the most favorable cases it is possible to observe in the electronic absorption spectrum transitions between these two states which allow the direct measurement of *B*. It must be stressed at this point that magnetic measurements alone cannot allow the measurements of *J* and *B* separately, since, at best, one can measure the energy difference between the ground state and a few of the low-lying excited states which all belong to the same solutions (+ or −).

Another feature characterizing the mixed valence systems is the so-called *valence trapping*. The mixed valence systems are traditionally[12] divided into three classes according to the extent of the delocalization of the electron which is formally added to the integer valence complex to obtain the mixed valence one. This *extra* electron can be completely delocalized over both metal centers (class III) or completely localized onto one of them (class I). Class II compounds have an intermediate behavior which often leads to a temperature-dependent localiza-

[†] Università di Napoli.
[‡] Università di Firenze.
[§] Université de Fribourg.

(1) *Mixed Valence Compounds*; Brown, D. B., Ed.; Reidel: Dordrecht, 1980.
(2) *Electron Transfer in Biology and the Solid State*; Johnson, K. M., King, R. B., Kurtz, D. M., Jr., Kutal, C., Norton, M. L., Scott, R. A., Eds.; ACS Advances in Chemistry Series; American Chemical Society: Washington, DC, 1990; Vol. 226.
(3) *Mixed Valence Systems: Applications in Chemistry, Physics and Biology*; Prassides, K., Ed.; Kluwer Academic Publishers: Dordrecht, 1991.
(4) Kahn, O. In *Magnetic Molecular Materials*; Gatteschi, D., Kahn, O., Miller, J. S., Palacio, F., Eds.; Kluwer Academic Publishers: Dordrecht, 1991; Vol. 198, p 35.
(5) *Iron−Sulfur Proteins*; Cammack, R., Ed. *Adv. Inorg. Chem.* **1992**, *38*.
(6) Solomon, E. I. In *Metal Clusters in Proteins*; Que, L., Jr., Ed.; ACS Symposium Series; American Chemical Society: Washington, DC, 1988.
(7) *Manganese Redox Enzymes*; Pecoraro, V. L., Ed.; VCH Publishers: New York, 1992.
(8) Zener, C. *Phys. Rev.* **1951**, *82*, 403.
(9) Anderson, P. W.; Hasegawa, H. *Phys. Rev.* **1955**, *100*, 675.
(10) Blondin, G.; Girerd, J.-J. *Chem. Rev.* **1990**, *90*, 1359.
(11) Kahn, O. *Molecular Magnetism*; VCH Publishers: New York, 1993.
(12) Robin, M. B.; Day, P. *Adv. Inorg. Chem. Radiochem.* **1967**, *10*, 247.

S0002-7863(97)03497-5 CCC: $15.00 
Published on Web 08/08/1998

tion. The classification of the mixed valence systems requires a lot of detailed spectromagnetic experiments, like EPR, magnetization measurements, and Mössbauer spectroscopy as a function of temperature. In the field of computational modeling of molecular magnetism aiming to rationalize observed magnetic behavior and/or to predict new ones, both semiempirical and/or first principle calculations are currently applied.[11,13] Well-established magnetostructural correlations are in fact generally used to design new molecular materials with predictable magnetic properties.[14] Far less is known about the spin-dependent electron delocalization mechanism except that it is strongly related to the coupling of electronic and nuclear motions and that overlap between magnetic orbitals is required in order to favor the electronic delocalization.[15,16]

The pioneering paper[17] by Noodleman and Baerends gave the basis of a general formalism which can be applied to handle both exchange and double exchange interactions, and this formalism, which we call the broken symmetry (BS) approach, has been applied to compute the *J* and *B* parameters in systems as complex as cubane-like iron sulfur clusters.[18] This model of calculation, which is applicable for weakly coupled systems only, is based on the projection of the energy of a single determinant of broken space and spin symmetry onto the energies of pure spin multiplets. A separate calculation of the energy of the highest spin multiplicity state (which can be reasonably well represented with a single Slater determinant) allows one to compare the difference in energies obtained by molecular orbital calculations with those given by eq 1 and then to compute the spin Hamiltonian parameters. Since the systems which have been considered are large molecular systems, the BS approach has been mostly applied[18] within the density functional (DF) theory,[19] although Hartree−Fock (HF) calculations have also been applied as well on some binuclear systems with integer valence.[20,21] We recently proposed a model which is applicable in the case of strongly coupled systems as well.[20,22]

The modeling of valence trapping phenomena, which is required in order to have a deeper insight into the electronic structure of mixed valence compounds, requires the knowledge of the potential energy surface of the system as a function of the position of the atomic nuclei. Since rather small geometrical variations (∼0.1 Å in bond distances and ∼1° in bond angles) can be indicative of valence trapping, a method of calculation is needed which can reproduce the energy changes upon small nuclear displacements with sufficient accuracy and which can be applied to large molecular systems containing transition metal ions. Recently DF theory has been used to reproduce the energy surface[23] of the complex $VCl_4$, which undergoes a dynamic Jahn−Teller effect, and that of $Cr_2$.[24]

We have applied the density functional theory[19] using the broken symmetry approach[18] to compute the spectromagnetic properties of $[Fe_2(OH)_3(tmtacn)_2]^{2+}$, modeled by replacing the tmtacn ligand (*N*,*N*′,*N*″-trimethyl-1,4,7-triazacyclononane) by three ammonia molecules, and to compute its potential energy surface as a function of the Fe−Fe distance following a path of minimal energy. The complex cation[25,26] $[Fe_2(OH)_3(tmtacn)_2]^{2+}$ can be considered as a rare example of a mixed valence Fe(II)−Fe(III) system with full valence delocalization (class III) related to binuclear iron sulfur sites found in the active sites of ferredoxins.[27] It has a $S = 9/2$ state strongly stabilized with respect to other spin states, and its physicochemical properties are still being actively studied. Recently an accurate experimental characterization of the ground and low excited states has been performed.[28,29] This characterization includes, among others, the determination of the energy difference between the ground state and the first excited one and the measurement of single crystal polarized electronic spectra and the vibronic distortions of the first excited state. This system seems therefore particularly well suited to test the ability of DF theory to reproduce the electronic structure of mixed valence systems including the calculation of adiabatic potential energy surfaces. These are the results we report in this paper.

## Computational Details

Electronic calculations were performed with the Amsterdam density functional (ADF) program package, version 2.2.[30,31] The standard basis sets provided within the package were used throughout. Double-ζ STO basis sets were applied to the valence electrons of all non-hydrogen atoms, except the iron 3d orbitals which were represented using a triple-ζ function. The shells up to 3p for Fe and 1s for all the other non-hydrogen atoms were treated as frozen cores. Single-ζ STO basis sets were used for hydrogen atoms.

In preliminary calculations various approximations to the exchange correlation potential were used. The VWN−Stoll approximation to the exchange correlation potential includes the local potential of Vosko, Wilk, and Nusair[32] with added the Stoll's correlation[33] correction term. Gradient corrections to the exchange and correlation potentials were applied in the form proposed by Becke[34] for the exchange part and by Perdew[35] for the correlation, or using the more recent Perdew and Wang[36] exchange correlation corrections. The VWN−Stoll approximation was used in all the other calculations for the reasons explained below.

(13) (a) Miralles, J.; Daudey, J. P.; Caballol, R. *Chem. Phys. Lett.* **1992**, *198*, 555. (b) Miralles, J.; Castell, O.; Caballol, R.; Malrieu, J. P. *Chem. Phys.* **1993**, *172*, 33. (c) Castell, O.; Miralles, J.; Caballol, R. J. P. *Chem. Phys.* **1994**, *179*, 377. (d) Wang C.; Fink K.; Staemmler V. *Chem. Phys.* **1995**, *201*, 87. (e) Fink K.; Fink R.; Staemmler V. *Inorg. Chem.* **1994**, *33*, 6219.

(14) *Magnetic Molecular Materials*; Gatteschi, D., Kahn, O., Miller, J. S., Palacio, F., Eds.; Kluwer Academic Publishers: Dordrecht, 1991; Vol. 198, p 35.

(15) Borshch, S. A., Bominaar, E. L.; Blondin, G.; Girerd, J.-J. *J. Am. Chem. Soc.* **1993**, *115*, 5155.

(16) Bominaar, E. L.; Hu, Z.; Münck, E.; Girerd, J.-J.; Borshch, S. A. *J. Am. Chem. Soc.* **1995**, *117*, 6976.

(17) Noodleman, L.; Baerends, E. J. *J. Am. Chem. Soc.* **1984**, *106*, 2316.

(18) Noodleman, L.; Peng, C. Y.; Case, D. A.; Mouesca, J.-M. *Coord. Chem. Rev.* **1995**, *144*, 199.

(19) Parr, R. G.; Young, W. *Density Functional Theory of Atoms and Molecules*; Oxford University Press: New York, 1989.

(20) Bencini, A.; Totti, F.; Daul, C. A.; Doklo, K.; Fantucci, P.; Barone, V. *Inorg. Chem.* **1997**, *36*, 5022.

(21) (a) Hart, J. R.; Rappé, A. K.; Gorun, S. M.; Upton, T. H. *J. Phys. Chem.* **1992**, *96*, 3654. (b) Hart, J. R.; Rappé, A. K.; Gorun, S. M.; Upton, T. H. *J. Phys. Chem.* **1992**, *96*, 6264. (c) Hart, J. R.; Rappé, A. K.; Gorun, S. M.; Upton, T. H. *Inorg. Chem.* **1992**, *31*, 5254.

(22) Daul, C. *Int. J. Quantum Chem.* **1994**, *52*, 867.

(23) Bruyndonckx, R.; Daul, C.; Manoharan, P. T.; Deiss, E. *Inorg. Chem.* **1997**, *36*, 4251.

(24) Edgecombe, K. E.; Becke, A. D. *Chem. Phys. Lett.* **1995**, *244*, 427.

(25) Drüecke, S.; Chaudhuri, P.; Pohl, K.; Wieghardt, K.; Ding. X.-Q.; Bill. E.; Sawaryn, A.; Trautwein, A. X.; Winkler, H.; Gurman, S. J. *J. Chem. Soc., Chem. Commun.* **1989**, 59.

(26) Ding. X.-Q.; Bominaar, E. L.; Bill. E.; Winkler, H.; Trautwein, A. X.; Drüecke, S.; Chaudhuri, P.; Wieghardt, K. *J. Chem. Phys.* **1990**, *92*, 178.

(27) Papaefthymiou, V.; Girerd, J.-J.; Moura, I.; Moura, J. J. G.; Münck, E. *J. Am. Chem. Soc.* **1987**, *109*, 4703.

(28) Gamelin, D. R.; Bominaar, E. L.; Mathonière, C.; Kirk, M. L.; Wieghardt, K.; Girerd, J.-J.; Solomon, E. I. *Inorg. Chem.* **1996**, *35*, 4323.

(29) Gamelin, D. R.; Bominaar, E. L.; Kirk, M. L.; Wieghardt, K.; Solomon, E. I. *J. Am. Chem. Soc.* **1996**, *118*, 8085.

(30) ADF 2.2, ADF 2.3, Theoretical Chemistry, Vrije Universiteit, Amsterdam.

(31) (a) Baerends, E. J.; Ellis, D. E.; Ros, P. *Chem. Phys.* **1973**, *2*, 41. (b) te Velde, G.; Baerends, E. J. *J. Comput. Phys.* **1992**, *99*, 84.

(32) Vosko, S. H.; Wilk, L.; Nusair, M. *Can. J. Phys.* **1980**, *58*, 1200.

(33) Stoll, H.; Pavlidou, C. M. E.; Preuss, H. *Theor. Chim. Acta* **1978**, *49*, 143.

(34) Becke, A. D. *Phys. Rev. A* **1988**, *38*, 3098.

(35) Perdew, J. P. *Phys. Rev. B* **1986**, *33*, 8822.

**Table 1.** Relevant Geometrical Parameters of $[Fe_2(OH)_3(NH_3)_6]^{2+}$ Obtained by Geometry Optimization

| geometrical parameters | VWN−Stoll[a] | B[b] | PW91[c] | BPW91[d] | VWN−Stoll[e] | exptl[f] |
|---|---|---|---|---|---|---|
| Fe−Fe (Å) | 2.51 | 2.68 | 2.57 | 2.58 | 2.53 | 2.51 |
| Fe−O (Å) | 2.01 | 2.10 | 2.04 | 2.04 | 2.02 | 1.94 |
| O−H (Å) | 1.02 | 1.02 | 1.01 | 1.01 | 1.02 | |
| Fe−O−Fe (deg) | 77.2 | 79.0 | 78.1 | 78.2 | 77.6 | 80.4 |
| O−Fe−O (deg) | 85.2 | 83.8 | 84.5 | 84.5 | 84.9 | 82.8 |

[a] Local density functional of Vosko−Wilk−Nusair[32] with Stoll's correction[33] for the correlation. [b] VWN−Stoll with nonlocal Becke's corrections[34] for the exchange part. [c] VWN with the nonlocal Perdew−Wang exchange correlation potential.[36] [d] VWN with Becke nonlocal exchange and Perdew−Wang correlation potential.[36a] [e] VWN−Stoll geometry optimization without constrains. The optimized values for Fe−N and Fe−Fe−N are Å and 126°, respectively. The ammonia molecules were assigned a tetrahedral symmetry with N−H = 1.0 Å. [f] From ref 29.

Anharmonic frequencies needed for the estimation of vibronic couplings (vide infra) were computed with the DiNa package.[37]

**Choice of the Functional.** Sometimes the application of DF theory to chemical problems seems to turn into a form of a roulette in which one tries a long list of functionals; compare the results obtained in this way and choose different functionals for different molecules according to the agreement one obtains with the experiment, case by case. Magnetic exchange coupling constants in oligonuclear transition metal complexes, organic biradical, and coupled transition metal−organic radical systems have now been computed using several approaches, and a comparison between the various methods on selected compounds has appeared.[20] When the exchange coupling constants are computed through the BS approach,[18] which is briefly summarized in the next section, much of the electron correlation of low spin state is included in the BS determinant[18] and the best agreement with the experiment is obtained using the noncorrelated Xα functional[39] or the VWN one.[32] Gradient corrections always lead to an overestimation of the correlation and to a larger singlet−triplet gap. Also inclusion of Stoll's correction for the correlation between electrons with the same spin[33] gave significant improvements to the result. It seems, therefore, that for the calculation of the magnetic structure the use of the local functionals is a general purpose recipe. In the case of mixed valence systems it is important to compute geometries which are as near as possible to the experimental ones, and we have therefore also applied gradient-corrected methods to investigate the influence of nonlocal corrections to the exchange correlation functional on the computed geometries. The results of the calculations are presented in Table 1 and discussed in the next section. The geometries computed with the VWN−Stoll functional are in better agreement with the experiments, and as a consequence, also the $\sigma \rightarrow \sigma^*$ (see the next section for a complete definition), which is used to compute the double exchange parameter $B$ and strongly depends on the Fe−Fe bond distance, is better reproduced using the VWN−Stoll functional. The VWN functional has also been successfully applied by Stranger et al. to characterize a number of face-shared dimers of different transition metals.[38]

Due to these considerations, the effect of nonlocal corrections on the calculation of properties other than geometries has not been investigated and the VWN−Stoll functional was used for all the calculations.

## Results and Discussion

**Spectromagnetic Properties.** The calculations were performed on a model molecule, already used for Xα-SW calculations,[29] in which the tridentate tmtacn ligand was substituted by three ammonia molecules. The model molecule, $[Fe_2(OH)_3(NH_3)_6]^{2+}$, and the relevant geometrical parameters used in the calculations are shown in Figure 1. To take into account the rigidity and steric requirement imposed on the molecule by the macrocyclic ligand, the geometry of the ammonia groups around the iron atoms was kept fixed with Fe−N = 2.21 Å and Fe−Fe−N = 130°, which are averaged values from the bond distances and angles found in the crystal structure.[29] This approximation was used for all the calculations of the spectroscopic observables and agrees with the experimental IR and resonance Raman data which show that only the relative motion of the Fe and OH groups contributes to the intervalence charge-transfer transition.[28] All the spectroscopic observables did not show[29] deviations from the idealized $D_{3h}$ symmetry; hence, this symmetry will be used in the following, unless when BS calculations are performed. In these cases the irreducible representations of the $C_{3v}$ point group will be used to label the molecular orbitals. The geometries optimized with the above constraints on the high spin $S = 9/2$ state using different functionals are compared in Table 1. The result of a full geometrical optimization with the VWN−Stoll functional[32,33] is also shown. Inclusion of nonlocal corrections leads to larger Fe−Fe distances as compared to the experimental values. All the following results were obtained using the VWN−Stoll functional,[32,33] for the reasons explained in the previous section. The structure obtained by the full geometry optimization also agrees rather well with the experimental findings, except for a distortion of the Fe−Fe−N angle to a lower value which is probably not allowed by the macrocyclic ligand.

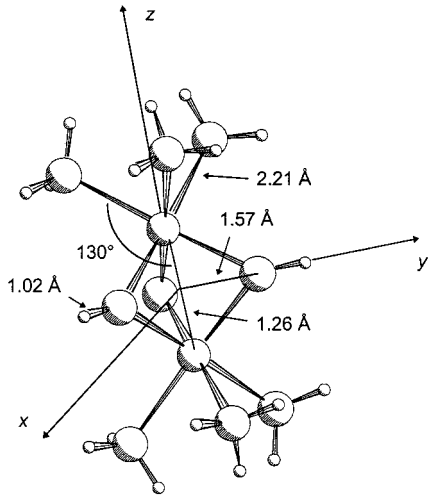


**Figure 1.** Schematic view of the model cation $[Fe_2(OH)_3(NH_3)_6]^{2+}$ showing the reference system and the internal coordinates used in the geometrical optimizations. The numerical values correspond to the constrained optimization in which the Fe−N distance and the Fe−Fe−N angle were fixed (see the text).

The one-electron energy levels computed for $[Fe_2(OH)_3(NH_3)_6]^{2+}$ in the high spin state $S = 9/2$ are shown in Figure 2. The 11 α spin electrons are occupying orbitals which are mainly composed by 3d iron orbitals, except the orbital $2a_2'$ which is a linear combination of in-plane 2p orbitals of the oxygen atoms. The highest occupied $\beta$ orbitals correspond to $2a_2'$ and $6a_1'$, yielding a total of 9 unpaired electrons. In Table 2 we report the gross atomic orbital populations of α 3d metal orbitals forming the SOMOs, and that of the doubly occupied orbital $6a_1'$. We briefly call an orbital doubly occupied when both the α and the $\beta$ spin−orbitals contain one electron. The $6a_1'$ orbital is the in-phase linear combination of the $z^2$ orbitals of both Fe

(36) (a) Perdew, J. P.; Wang, Y. *Phys. Rev. B* **1986**, *33*, 8800. (b) Perdew, J. P.; Chevary, J. A.; Vosko, S. H.; Jackson, K. A.; Pederson, M. R.; Singh, D. J. *Phys. Rev. A* **1992**, *46*, 6671.

(37) Barone, V. In *Recent Advances in Density Functional Methods*; Chang, D. P., Ed.; World Scientific: Singapore, 1996; Vol. 1, p 287.

(38) McGrady, J. E.; Stranger, R.; Lovell, T. *J. Phys. Chem.* **1997**, *101*, 1A, 6265.

(39) Slater, J. C. *Quantum Theory of Molecules and Solids*; McGraw-Hill: New York, 1974; Vol. 4.

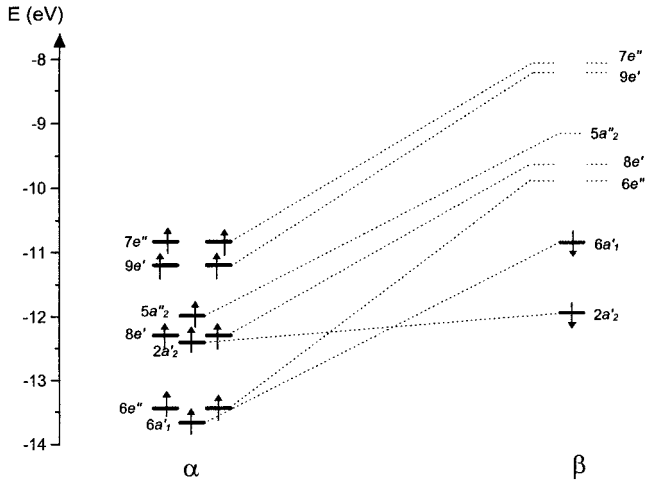


**Figure 2.** Spin unrestricted molecular orbitals near the Fermi level computed for the ground state $^{10}A_2''$.

**Table 2.** 3d Percent Gross Populations[a] of the One-Electron α and β Orbitals in the Region HOMO−LUMO[b]

| symmetry/orbital | $z^2$ | $xz$ | $yz$ | $xy$ | $x^2-y^2$ |
|---|---|---|---|---|---|
| 7e″ | 0 | 0 | 31 (54) | 17 (23) | 0 |
| 9e′ | 0 | 48 (63) | 0 | 0 | 10 (18) |
| $5a_2''$ | 69 (92) | 0 | 0 | 0 | 0 |
| 8e′ | 0 | 3 (16) | 0 | 0 | 33 (67) |
| 6e″ | 0 | 0 | 38 (34) | 44 (64) | 0 |
| $6a_1'$ | 94 (95) | 0 | 0 | 0 | 0 |

[a] Only one component of the doubly degenerate species is shown. The d orbitals span the following irreducible representations in $D_{3h}$: $z^2_+ \in a_1'$, $z^2_- \in a_2''$, $z^2_+ \in a_1'$, $(x^2-y^2_+, xy_+) \in e'$, $(xz_-, yz_-) \in e'$, $(xy_-, x^2-y^2_-) \in e''$, $(yz_+, xz_+) \in e''$, where + and − indicate the sign of the linear combinations of the orbitals on the two iron centers. [b] The occupation of the α orbitals is always 1. The occupation of the $6a_1'$ β orbital is 1; the other β orbitals are unoccupied (see Figure 2). The populations of the β orbitals are in parentheses.

centers and, as already noted by Solomon et al.,[29] this strongly metal−metal bonding orbital is almost completely localized onto the two metals with a small contribution from in-plane 2p orbitals of the oxygens. The antibonding counterpart is $5a_2''$ and it is singly occupied. In this molecular orbital the $z^2$ orbitals can interact with the $2p_z$ oxygen orbitals, which are perpendicular to the $O_3$ plane, and the computed gross atomic orbital population is consequently smaller (69% vs 94%). The e-type orbitals are rather strongly interacting with the oxygen orbitals and are responsible for the superexchange contributions to the magnetic interaction between the metals.

Two high spin $S = 9/2$ states can arise according to the double occupation of the $6a_1'$ or $5a_2''$ orbitals, respectively. These two states can be identified as the two components $E_{\pm}(9/2)$ of the spin Hamiltonian solution (eq 1), whose energy difference is, therefore, 10*B*. The electronic transitions were computed using the Slater transition state formalism[39] in $C_{2v}$ symmetry (with the $C_2$ axis perpendicular to the Fe−Fe bond) in order to distinguish between the orbitals belonging to degenerate (e) representations of the $D_{3h}$ point group. The results of the calculations are shown in Table 3. The transition energies are in general agreement with the experimental ones and with those previously obtained by Xα-SW calculations.[29] The computed energy for the transition $6a_1' \rightarrow 5a_2''$, which we can call also $\sigma \rightarrow \sigma^*$, is very close to the experimental value, while all the calculations suggest a reverse ordering for the two high-energy bands. From the energy of the transition $6a_1' \rightarrow 5a_2''$ we compute $B = 1366$ cm$^{-1}$ to be compared with the experimental value of 1350 cm$^{-1}$.

**Table 3.** Computed One-Electron Transition for $[Fe_2(OH)_3(NH_3)_6]^{2+}$ (cm$^{-1}$)

| one-electron excitation | assignment[a] | Xα-SW[b] | calcd | exptl[b] |
|---|---|---|---|---|
| $6a_1' \rightarrow 6e''$ | $^{10}A_2'' \rightarrow {}^{10}E''$ [c] | 6 380 | 8 388 | |
| $6a_1' \rightarrow 8e'$ | $^{10}A_2'' \rightarrow {}^{10}E'(x,y)$ | 10 719 | 10 987 | 7 380 |
| $6a_1' \rightarrow 5a_2''$ | $^{10}A_2'' \rightarrow {}^{10}A_1'(z)$ | 13 300 | 13 660 | 13 500 |
| $6a_1' \rightarrow 7e''$ | $^{10}A_2'' \rightarrow {}^{10}E''$ [c] | 25 011 | 22 712 | 17 860 |
| $6a_1' \rightarrow 9e'$ | $^{10}A_2'' \rightarrow {}^{10}E'(x,y)$ | 23 204 | 21 207 | 21 350 |

[a] Polarizations of the transitions are given in parentheses. [b] From ref 29. [c] Symmetry forbidden in $D_{3h}$.

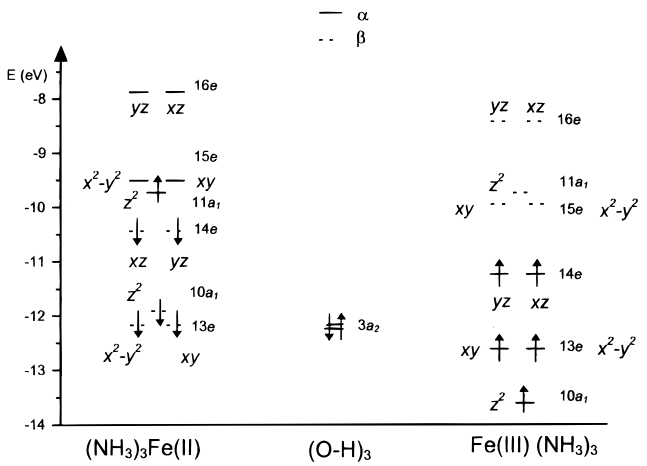


**Figure 3.** Molecular orbitals near the Fermi level computed on the broken symmetry state. The orbitals are grouped according to the prevalent localization on the formally Fe(II) center (left), the formally Fe(III) center (right), and the $(OH)_3$ group (center). β spin−orbitals have dotted lines. The levels are labeled according to $C_{3v}$ symmetry (see the text). The $z^2$ orbitals are delocalized onto the two metals (see the text). In the figure they have been left near the two metals to preserve the formal oxidation state of the ions.

The calculation of the exchange coupling constant, *J*, appearing in eq 1 requires the knowledge of the energy of a spin state with spin multiplicity *S* different from 9/2. The description of low spin states generally requires the use of state functions which are linear combinations of Slater determinants and therefore cannot be handled within conventional DFT.[19] We handled this situation by the BS formalism which employs the energy of a reference state of mixed spin and space symmetry, the BS state, obtained by imposing two high spin states on the different iron centers with opposite spins.[18] The key equation which allows the calculation of *J* is

$$E_{av}(S_{max}) - E(BS) = 2JS_AS_B \qquad (2)$$

where $E_{av}(S_{max})$ is the average of the energies of the high spin states obtained through the transition $\sigma \rightarrow \sigma^*$ via two separate SCF calculations, $E(BS)$ is the energy of the BS state, and $S_A$ and $S_B$ are the maximum spins on the two metal centers. In the present case the BS determinant represents a state with $M_S = 1/2$ ($M_{S_A} = -2$, $M_{S_B} = 5/2$). Equation 2 gives $E_{av}(9/2) - E(BS) = 10J$, from which we get $J = 137$ cm$^{-1}$.

The BS orbitals are generally taken as good representations[18,20] for the *natural magnetic orbitals* in weakly coupled systems and are widely used for a qualitative understanding of the magnetic interactions in terms of their overlap.[11] When the magnetic orbitals can overlap in a significant region of space, they give rise to an *antiferromagnetic pathway*, while if they are orthogonal, but still have regions of space in which the

(40) Bencini, A. *J. Chim. Phys. Phys.-Chim. Biol.* **1989**, *86*, 763.

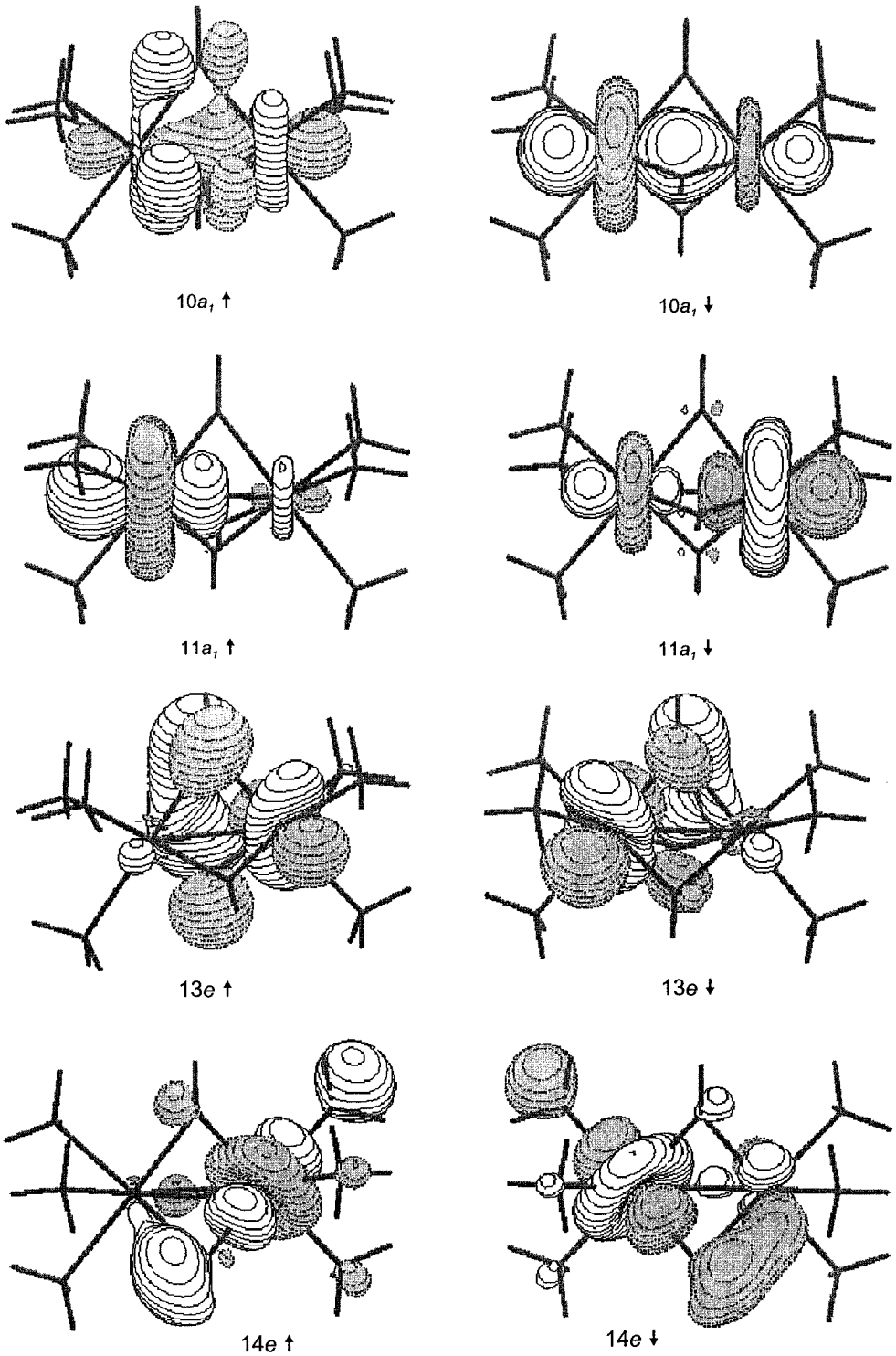


**Figure 4.** Isovalue representation of (a, top two rows) BS molecular orbitals spanning the $a_1$ irreducible representation and (b, bottom two rows) BS molecular orbitals spanning the e irreducible representation. The surface drawn corresponds to $\psi = 0.1(e\ a_0^{-3})^{1/2}$. The Fe(II) center is the iron atom on the left of the dinuclear system.

differential overlap is nonzero, they give rise to a *ferromagnetic pathway*.[41] The BS orbitals are localized onto the two different halves of the molecule depending on the overlap between the orbitals forming the symmetric and antisymmetric molecular orbitals. Strong overlap causes a small localization and indicates the presence, e.g., of a direct metal−metal interaction. The molecular orbitals in the SOMO region obtained from the BS calculation, which have mainly a 3d metal character, are shown in Figure 3. The symmetry labels are that of the $C_{3v}$ symmetry group and correlate with those of $D_{3h}$ according to $(a_1', a_2'') \rightarrow a_1$; $(a_1'', a_2') \rightarrow a_2$; $(e', e'') \rightarrow e$. In Figure 3 the orbitals are grouped according to their main localization on the left iron center (spin population −3.21; formally Fe(II)) and the right iron center (spin population 3.91; formally Fe(III)) or on the central OH groups. The doubly occupied $3a_2$ orbital is a nonbonding linear combination of $2p_y$ and $2p_x$ orbitals localized on the center of the molecule; the other orbitals are more or

(41) (a) Kahn, O.; Charlot, M. F. *Nouv. J. Chim.* **1980**, *4*, 567. (b) Charlot, M. F.; Kahn, O.; Bencini, A.; Gatteschi, D.; Zanchini, C. *Inorg. Chem.* **1986**, *25*, 1060.

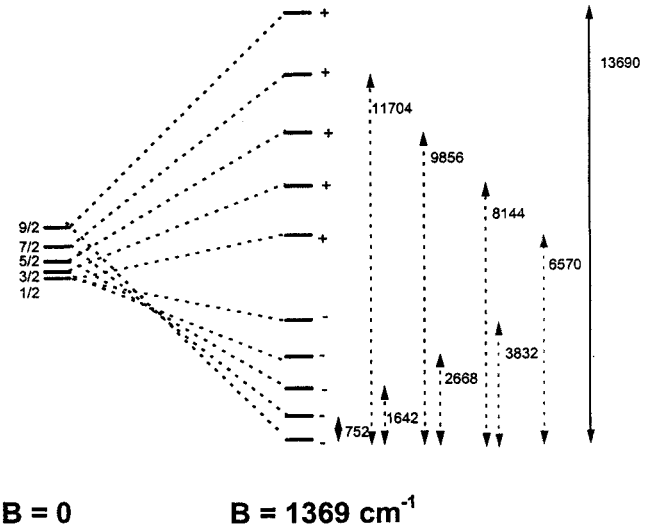


**Figure 5.** Energy of the spin state computed using eq 1 with $J = 137$ cm$^{-1}$ and $B = 0$ (left) and $J = 137$ cm$^{-1}$ and $B = 1366$ cm$^{-1}$ (right).

less localized on the two halves of the molecule, including the ammonia groups. A *pseudo*tridimensional representation of the $a_1$ and e molecular orbitals is shown in Figure 4.[42] The $a_1$ orbitals include the doubly occupied $10a_1$ orbital, which is the *in-phase* combination of the $z^2$ metal orbitals. The orbital is not well localized as a consequence of the strong overlap between the atomic orbitals, which is responsible for a net metal−metal bond. The couple of $11a_1$ spin−orbitals (singly occupied with spin $\alpha$) are better localized on the two metal centers with the $\alpha$ electron more localized on the Fe(II) center. The e orbitals are well localized onto the different metal centers with significant contributions on the bridging OH groups, thus contributing to the superexchange mechanisms. A significant overlap occurs between the magnetic orbitals through the oxygen atoms, suggesting antiferromagnetic superexchange pathways which must be more efficient between the 13e pair of spin−orbitals.

Using eq 1 and the calculated values of $J$ and $B$, we obtain the relative ordering of the spin multiplets shown in Figure 5. On the left-hand side the energy level ordering for $B = 0$ is shown. The low spin state $S = 1/2$ is the ground state as a consequence of the overall antiferromagnetic exchange interaction. The effect of the double exchange interaction, through the parameter $B$, is that of stabilizing the high spin state $S = 9/2$. The next spin state, $S = 7/2$, lies 752 cm$^{-1}$ higher in energy, in good agreement with the measured temperature dependence of the magnetic susceptibility which indicates a lower limit of 720 cm$^{-1}$ for the energy separation between the $S = 7/2$ and $S = 9/2$ spin states.[29] It is worth noting that experimental techniques do not allow the separate measure of $J$ and $B$. It is therefore of importance to have a method of calculation of $J$ which can give an independent estimate of the exchange interaction.

Of course all the above discussion relies on a spin Hamiltonian formalism, which is the main model which experimentalists use to interpret magnetic properties of mixed valence systems. Direct comparison between a rigorously computed multiplet structure and experimental data would eliminate the use of the spin Hamiltonian parameters and the direct use of exchange and double exchange terms. Although this goal is quite ambitious, we are now developing a methodology for the direct calculation of the multiplet structure, which could lead to a validation of the spin Hamiltonian formalism itself.

(42) These plots have been obtained using the program MOLDEN, by G. Schaftenaar, properly modified to elaborate the ADF results by F. Mariotti, Dipartimento di Chimica, Università di Firenze.

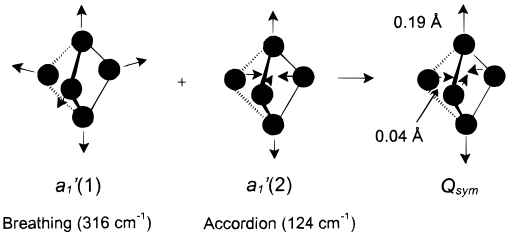


**Figure 6.** Normal vibrational modes of $a_1'$ symmetry and the $Q_{sym}$ coordinate associated with the $\sigma \rightarrow \sigma^*$ electronic transition.

**Table 4.** Relevant Geometrical Parameters for the $^{10}A_1'$ Excited State of $[Fe_2(OH)_3(NH_3)_6]^{2+}$ Obtained by Geometry Optimization

| geometrical parameters | exc state $^{10}A_1'$ | $\Delta(r)$ calcd | $\Delta(r)$ exptl[a] |
|---|---|---|---|
| Fe−Fe (Å) | 2.83 | 0.32 | 0.38 |
| Fe−O (Å) | 2.01 | 0.00 | 0.10 |
| O−H (Å) | 1.02 | 0.00 | |
| Fe−O−Fe (deg) | 87.7 | 10.5 | 9.4 |
| O−Fe−O (deg) | 77.3 | −7.88 | −7.1 |

[a] From refs 28 and 29.

**$6a_1' \rightarrow 5a_2''$ Excited State Distortion.** Using resonance Raman spectra, variable temperature band shape studies, and isotopic sensitivity effects, Solomon et al.[28,29] determined the nature of the distortion of the excited state generated by the transition $6a_1' \rightarrow 5a_2''$. The distortion does correspond to the symmetric linear combination of the totally symmetric in-phase *breathing* and out-of-phase *accordion* shown in Figure 6, yielding the $Q_{sym}$ normal mode. Note that this normal coordinate is the only one involving the stretching of the Fe−Fe bond. Nitrogen ligands gave only a negligible contribution to this vibration. The results of the geometry optimization of the excited state $^{10}A_1'$ arising from the excitation $6a_1' \rightarrow 5a_2''$ are reported in Table 4 and compared with the experimental data. The results can be considered satisfactory, also considering that no error estimate was given with the experimental data. The large error of the Fe−O distance (which is not directly used as a parameter in the geometrical optimization) is due to the additive effect of the errors in the Fe−Fe bond distance and in the bond angles. The experimental data reported in Figure 6 represent the deviations of the Fe and oxygen atoms from the equilibrium position in the ground state. The corresponding computed displacements are 0.16 and −0.10 Å.

**Adiabatic Potential Surfaces: High Spin State.** The ground state properties of the mixed valence systems depend on both static and dynamic mechanisms which determine the actual values of $B$ and $J$. The effect of nuclear displacements on the energies of the spin states obtained from eq 1 has been investigated, and a vibronic coupling mechanism in which the out-of-phase combination of the breathing motions on the two monomeric subunits, $Q_-$, has been claimed to be responsible for electron localization.[10] In the facial bioctahedral dimers this coordinate corresponds to an $a_2''$ normal mode in $D_{3h}$ symmetry, which becomes $a_1$ in $C_{3v}$ symmetry. The principal component of this nuclear displacement is the parallel shift of the $(OH)_3$ plane along the $C_3$ axis concomitant with an out-of phase variation of the metal−nitrogen distances. Since in the complex investigated experimentally the rigid macrocyclic ligands should reduce the importance of these latter displacements (as already observed for the other vibrational modes), we have exploited the potential surface of the system by displacing the $(OH)_3$ plane along the $z$ axis, keeping the Fe−Fe distance at the value of 2.512 Å and all the other geometrical parameters frozen. The

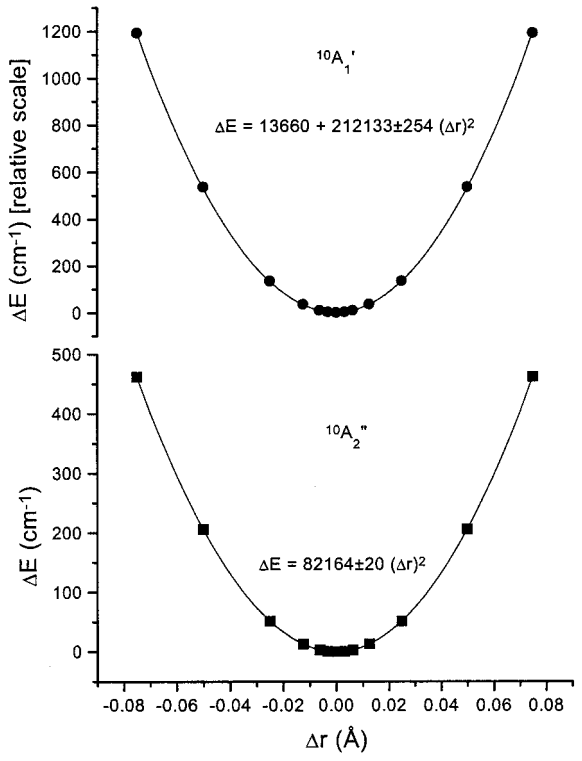


**Figure 7.** Dependence of the energy of the ground $^{10}A_2''$, $\sigma$, state (bottom) and of the $^{10}A_1'$, $\sigma^*$, excite state (top) on the displacement of the $(OH)_3$ plane from the origin along the *z* axis. The points have been obtained by constrained geometry optimization with Fe−Fe = 2.512 Å (see the text).

curve computed for the $S = 9/2$ ground state is shown in Figure 7. The points on the *x* axis represent the distance of the $(OH)_3$ plane from the origin, $\Delta r = 0$ corresponding to the symmetric $D_{3h}$ geometry in which the two Fe atoms have equal Fe−O distances. At each point of the curve we also computed the energy of the $\sigma^*$ excited state using the Slater transition state procedure.[39] The $\sigma^*$ potential energy curve is also shown in Figure 7. The points nicely follow a parabola in the form $y = a + bx^2$ (full line), indicating that the minimum in the energy function corresponds to a completely symmetrical dimer. The equation used for the upper curve contains the constant term $a = 13\,660$ cm$^{-1}$ which is the energy difference between the ground $^{10}A_2''$ and excited $^{10}A_1'$ states.

The curves reported in Figure 7 approximate the real potential surface as long as the hypothesis of a negligible contribution from the macrocycle is correct. To have a closer look at the influence of the nitrogen position on the molecular potential surface, we have performed geometry optimizations imposing only geometrical constraints on the ammonia groups (i.e., tetrahedral symmetry and N−H = 1.0 Å). The result of the optimization in $D_{3h}$ symmetry is shown in Table 1. Lowering the symmetry to $C_{3v}$ leads to a very similar geometry with the molecule still possessing an overall $D_{3h}$ structure. The relevant parameters for one iron center are Fe−O = 2.023 Å (1), Fe−N = 2.209 Å (0), O−Fe−O = 84.91° (3), nd Fe−Fe−N = 125.7° (−9). In parentheses we indicate the correction needed in obtaining the parameters for the other iron center. The optimized Fe−Fe distance is 2.53 Å, and the Fe−O−Fe angle is 77.5°. The geometry compares well with the experimental one except for the smaller Fe−Fe−N angles and the larger Fe−Fe distance. The small variation of the Fe−Fe distance has strong effects on the $\sigma \rightarrow \sigma^*$ transition, which is lowered to 13 000 cm$^{-1}$. These results show that the minimum in the

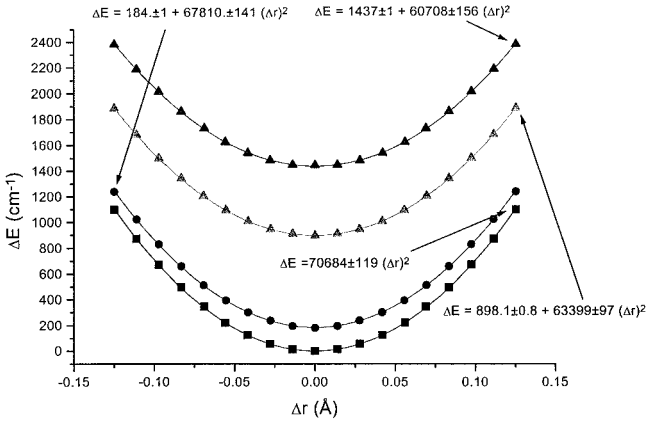


**Figure 8.** Minimal energy path of the ground $^{10}A_2''$ along the displacement of the $(OH)_3$ plane from the origin along the *z* axis. The points have been obtained by full geometry optimization with constrained Fe−Fe bonds at (from bottom to top) 2.53, 2.60, 2.70, and 2.75 Å (see the text).

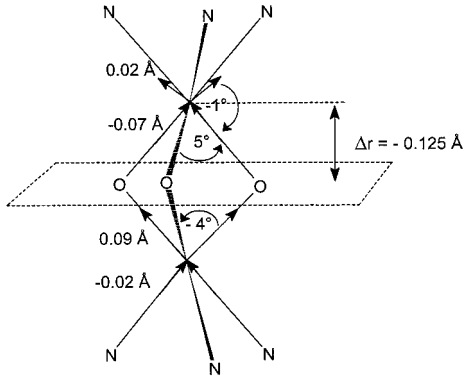


**Figure 9.** Computed geometrical variations upon displacement of the $(OH)_3$ plane of $|\Delta r| = 0.125$ Å.

energy surface still corresponds to a situation where the delocalization of the *extra* electron of the mixed valence couple is favored. To explore the energy surface to look for other relative minima, we computed the energy of the molecule by displacing the $(OH)_3$ plane toward one of the Fe centers and allowing the remaining part of the molecule to relax. In this way we followed the *minimum energy path* along the potential molecular surface. The results of the calculations are reported in Figure 8. A parabolic surface is still obtained characterized by a single minimum. Similar calculations were performed for Fe−Fe distances ranging from 2.53 to 2.75 Å. In any case only one minimum was found, indicating that the complete valence delocalization of the $^{10}A_2''$ state is not severely influenced by the metal−metal distances, but more by the topological arrangement of the bridging ligands. In Figure 9 the molecular rearrangement upon a displacement of the $(OH)_3$ plane, $|\Delta r| = 0.125$ Å, computed for the Fe−Fe distance of 2.53 Å is shown. The displacement is accompanied by small variations of the Fe−N bond distances and angles, while a larger deformation of the $Fe_2O_3$ core on the Fe−OH bond distances and O−Fe−O bond angles is computed. This deformation is close to the $a_2''$ ($Q_-$) vibrational normal mode.[28]

Although the previous results well agree with the experimental data, we found of interest to derive from them the parameters widely used to analyze the relative role of vibronic and double exchange effects. The second-order perturbative model used to this purpose[10,29] involves the ratio between the double exchange parameter ($B$) and the force constant ($k_-$) governing the motion along the antysymmetric normal mode

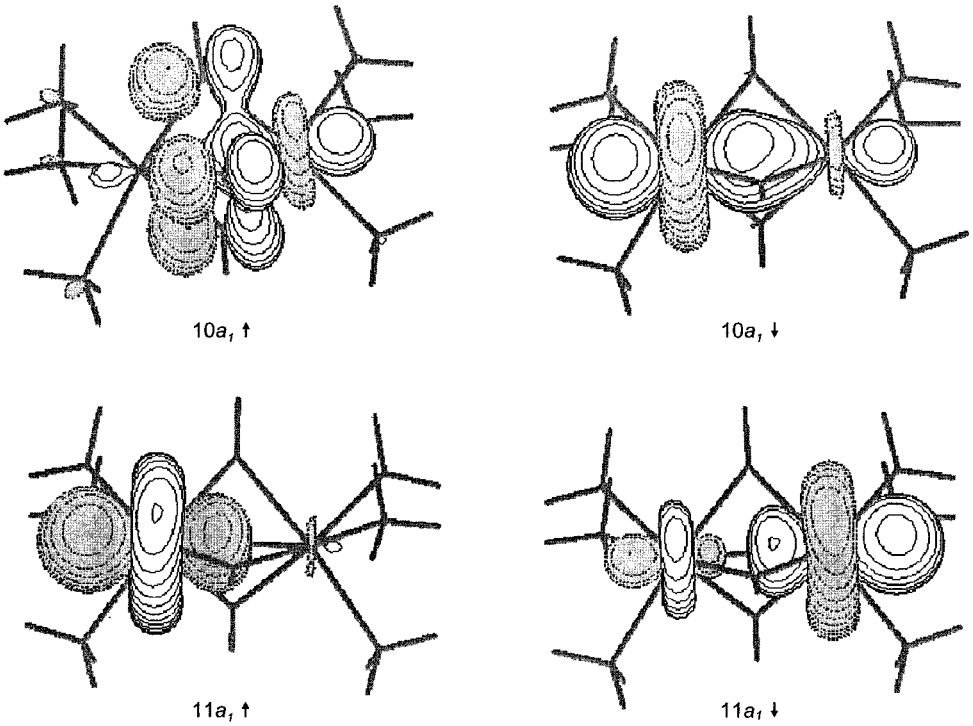


**Figure 10.** Isovalue representation of BS molecular orbitals spanning the $a_1$ irreducible representation computed for Fe−Fe = 2.70 Å. The surface drawn corresponds to $\psi = 0.1$ (e $a_0^{-3}$)$^{1/2}$. The Fe(II) center is the iron atom on the left of the dinuclear system.

($Q_-$) described above:

$$B\left(S+\frac{1}{2}\right)/\left(\frac{k_-^{\,2}}{2}\Delta Q_-\right) \qquad (3)$$

In turn, the normal coordinate $Q_-$ can be recast in terms of the average difference between metal−ligand bond lengths in oxidized and reduced monomeric units ($\Delta r \cong 0.1$ Å from literature values[29,43]), the average mass of the ligand surrounding the metal ($\mu = 15.5$ g mol$^{-1}$, average of 3N + 3OH), their number ($n = 6$), and a dimensionless coordinate $x_-$:

$$\Delta Q_- = \sqrt{\mathrm{nm}}\Delta r x_- \qquad (4)$$

The only parameter to be determined is, therefore, $k_-$ or, equivalently, the frequency $\nu_-$ governing the motion along $Q_-$, since $k_- = 4\pi^2c^2\mu\nu_-$. In ref 29 this quantity was estimated as 306 cm$^{-1}$ from literature values.[28] We can, however, directly compute this value by a proper analysis of the potential energy curves described above. In particular, computation of the distance in the mass-weighted coordinate between the structures built by linear synchronous transit or constrained optimization leads to an effective one-dimensional Schrödinger equation for the motion of a particle with a unitary mass.[44] This equation can be numerically solved by a numerical spline approach[37] to give anharmonic frequencies for this motion. Of course, the structures issuing from electronic calculations must be properly oriented in order to eliminate spurious rotational components.[45] All these steps are fully automated in the program package DiNa.[46] The results show that the motion is essentially harmonic (the difference between actual frequencies and their harmonic approximation being lower than 5 cm$^{-1}$). Vibrational frequencies ranging between 360 and 330 cm$^{-1}$ depending on the model used (rigid displacement of the $(OH)_3$ plane or constrained geometry optimization) were computed. The agreement with the experimental estimate[28] of 306 cm$^{-1}$ paves the route to the completely a priori determination of all of the parameters ($J$, $B$, $\nu_-$) entering the phenomenological Hamiltonian describing the electronic structure of mixed valence dimers. Furthermore, the computed $\nu_-$ decreases to 210 cm$^{-1}$ for an Fe−Fe distance of 2.75 Å, indicating the onset of more important vibronic effects.

The calculation of the spin Hamiltonian parameters for Fe−Fe = 2.70 Å were performed as described above. The BS orbitals show a larger localization onto the two separate halves of the molecule, as shown in Figure 10 for the $a_1$ orbitals. This is due to the smaller overlap between the $z^2$ atomic orbitals. As a consequence the computed exchange coupling constant, $J = 23.8$ cm$^{-1}$, is smaller than the one calculated for Fe−Fe = 2.51 Å. Also the $\sigma \rightarrow \sigma^*$ transition is displaced to a lower energy, 8251 cm$^{-1}$, yielding $B = 825.1$ cm$^{-1}$. Using eq 1, we can see that the $S = 9/2$ state is still the ground state with the $S = 7/2$ spin manifold 717 cm$^{-1}$ higher in energy.

The above results indicate that for the facial bioctahedral Fe dimers a complete valence delocalization is expected for a wide range of Fe−Fe distances. This situation could be completely reversed for complexes with metals preceding Fe in the transition series which do not have the $z^2$ orbitals occupied (e.g., chromium dimers). We feel that the present approach can yield useful information if applied to investigate series of systems of this type.

## Conclusion

Density functional theory has been successfully applied to characterize the electronic structure and the magnetic properties of the mixed valence dinuclear complex $[Fe_2(OH)_3(tmtacn)_2]^{2+}$ modeled by replacing the tmtacn ligand with three ammonia molecules. The computed electronic transitions are in close

(43) Snyder, B. S.; Patterson, G. S.; Abrahamson, A. J.; Holm, R. H. *J. Am. Chem. Soc.* **1989**, *111*, 5214.
(44) Barone, V.; Minichino, C. *Theochem* **1995**, *330*, 325.
(45) Barone, V.; Adamo, C. *Chem. Phys. Lett.* **1995**, *241*, 1.
(46) DiNa Program, Release 2.1, by V. Barone, University of Naples.

agreement with the experimental values. The transition energies computed with the VWN−Stoll functional are closer to the experimental values than those previously computed with the Xα-SW method,[28] and both methods reverse the order of the two higher energy bands with respect to the experimental evidence. The present calculations also well reproduce the deformation of the molecule associated with the $\sigma \rightarrow \sigma^*$ transition. Minimum energy path calculations performed for several Fe−Fe distances suggest that the iron centers in the molecule are always equivalent, classifying this system as a class III mixed valence compound in agreement with the experimental observations. The present calculations also allowed a value of 137 $cm^{-1}$ to be estimated for the exchange coupling constant appearing in the spin Hamiltonian formalism used to describe experimentally the double exchange phenomenon. The overall ferromagnetic behavior observed for this complex arises therefore from the high value of the delocalization parameter $B =$ 1366 $cm^{-1}$, as shown in Figure 5. The value of 752 $cm^{-1}$ computed for the splitting of the first excited state is also in good agreement with magnetic measurements which posed a lower limit of 720 $cm^{-1}$ for this energy.[28] Increasing the Fe−Fe distance to 2.70 Å decreases the values of $J$ and $B$ to 23.8 and 825.1 $cm^{-1}$, respectively, but the ground state still remains $S = 9/2$ with the lowest spin state 717 $cm^{-1}$ higher in energy. It must be noted that this energy separation is in good agreement with the magnetic susceptibility, therefore stressing the fact that magnetic susceptibility alone cannot permit the unique determination of the $J$ and $B$ parameters.

The frequencies $\nu_-$ associated with the normal coordinate $Q_-$ responsible for the delocalization of the extra electron have also been computed in nice agreement with the experimental estimate. These calculations have shown for the first time that the harmonic approximation is valid for describing the motion of the system along $Q_-$ and open a new way of looking at the description of the electronic structure of mixed valence systems.

The present calculations which have been performed for the probably best characterized mixed valence system show that the DF formalism, using the VWN−Stoll functional, can give valuable information on the electronic structure of mixed valence compounds, also allowing the form of the ground state potential energy surface to be reproduced, which is extremely important for the proper modeling of the migration of the *extra* electron onto the molecular system. We are now planning to investigate with the same method less well characterized systems such as the Mn(III)−Mn(IV) couples which assume relevance in both biological and solid state chemistry.

JA973497U